Materials Science Forum
ISSN: 1662-9752, Vol. 1187, pp 87-98
doi:10.4028/p-3z29kF

Submitted: 2026-01-19
Revised: 2026-02-22
Accepted: 2026-02-23
Online: 2026-04-17

Influence of Variable Radius Die Geometry on Tube Bending: A Finite Element Parametric Study

Apostolos Aslanidis[1,a*], Jonas Reuter[1,b] and Bernd Engel[1,c]

[1]University of Siegen, Forming Technology Siegen (UTS), Breite Strasse 11, 57076 Siegen, Germany

[a]apostolos.aslanidis@uni-siegen.de, [b]jonas.reuter@uni-siegen.de, [c]bernd.engel@uni-siegen.de

Keywords: Profile Bending, Tube Bending, Profile Forming, Compression Bending, Variable Radius Die, Variable Bending Radius, Radial Gradient

Abstract. While bending processes for producing tube bends with a constant radius have been extensively investigated in recent years, only a limited number of studies have addressed form-bound bending processes for generating variable radii. In particular, a systematic investigation of the influence of bend die geometry with a variable radius profile on tool reaction forces, geometrical and non-geometrical bent part properties is still lacking. In this study, compression bending using bend dies with a continuously varying radius is investigated by means of finite element (FE) simulations. The geometry of the bend dies is parameterized using an Archimedean spiral curve, allowing the bending radius to be described as a function of the bending angle. The introduced radial gradient, defined as the derivative of the radius with respect to the bending angle, $dR/d\alpha$, serves as the central design parameter of the bend die and is systematically varied from constant radius with 0 mm/° to 1 mm/°. The influence of the radial gradient $dR/d\alpha$ of the bend die geometry on tool reaction forces as well as on the geometrical and non-geometrical properties of the bent part is investigated by means of a numerical parametric study for a selected bending task. The results show that for small to moderate values of $dR/d\alpha$, all investigated metrics exhibit a pronounced linear dependence on the radial gradient. This behavior is further confirmed by the evaluation of the maximum values of the process and geometric parameters as a function of $dR/d\alpha$, yielding high coefficients of determination (R^2). For larger values of $dR/d\alpha$, however, the sensitivity of both process-related and geometric characteristics decreases.

Introduction

Profile bending processes are classified into form-bound or die-dependent and kinematic or free-form methods [1, 2], or, equivalently, into processes using geometry-specific and generic tools [3, 4]. Furthermore, a distinction is made between continuous and incremental processes.

In free-form bending processes (e.g., TSS bending [5], three-roll push bending [6]), forming is achieved by controlled movement of the tools. As a result, the final part geometry is largely independent of the tool geometry. Adaptations to changing process conditions and part geometries can be implemented via the process kinematics. In contrast, form-bound processes (e.g., rotary draw bending or compression bending [7]) are limited by the predefined geometry of the forming tools. However, this form constraint enables extensive support of the workpiece, allowing the production of wrinkle-free parts with small radii and tight tolerances.

Due to their flexibility in process control, free-form tube and profile bending methods are particularly suitable for producing spline geometries. The target geometries are typically described using the Frenet-Serret formulas based on the moving Frenet-Serret frame, as shown among others by Groth et al. [6]. However, this continuous curve representation is often discretized into sections of constant radii to simplify execution of the bending process, see Groth et al. [6] and Wang et al. [8]. Following this, Engel et al. [9] present a method to discretize the spline geometries into segments of constant radii and directly derive the required machine parameters for three-roll push bending, also accounting for machine stiffness. Nevertheless, achieving the desired target geometry remains challenging, as transitions between radii induce complex mechanical and geometrical effects. For this reason, Groth et al. [6] developed a product planning system that anticipates such effects during the

design phase of the bent part. Furthermore, the reverse transformation of a bent part into a spline geometry, as part of quality control, presents a significant challenge. This issue is addressed by several studies, including Groth et al. [10] and Scandola et al. [11].

The application of form-bound bending processes to produce variable radii has received little attention in the scientific literature to date. One of the few examples is the work by Elyasi et al. [12], who conducted a phenomenological investigation of rotary draw bending using a bend die with a variable radius. In their study, the variable radius is defined as an involute curve. To further address this gap, the present study investigates the compression bending process with a variable radius through numerical simulation. In contrast to Elyasi et al. [12], the bend die geometry is defined by an Archimedean spiral curve. The radial gradient, defined as the derivative dR/dα, is systematically increased, and the resulting effects on tool reaction forces, geometrical and non-geometrical bent part properties are described both qualitatively and quantitatively.

The paper first outlines the compression bending process and the underlying simulation model. For a more detailed process description, reference is made to Tronvoll et al. [7]. The subsequent section presents the study design. This is followed by a detailed presentation of the results, which are then summarized, discussed, and used as a basis for further research perspectives.

Finite Element Model Setup

FE simulations are conducted using the explicit solver Ls-Dyna (version mpp d R 12.0.0) from Livermore Software Technology, LLC. The simulation model employed in this study is based on the FE model set up by Reuter [13, 14], which was experimentally validated for constant bending radii. In the present work, the model is extended to account for variable bending radii, enabling its application to virtual investigations. The model setup is illustrated in Fig. 1.

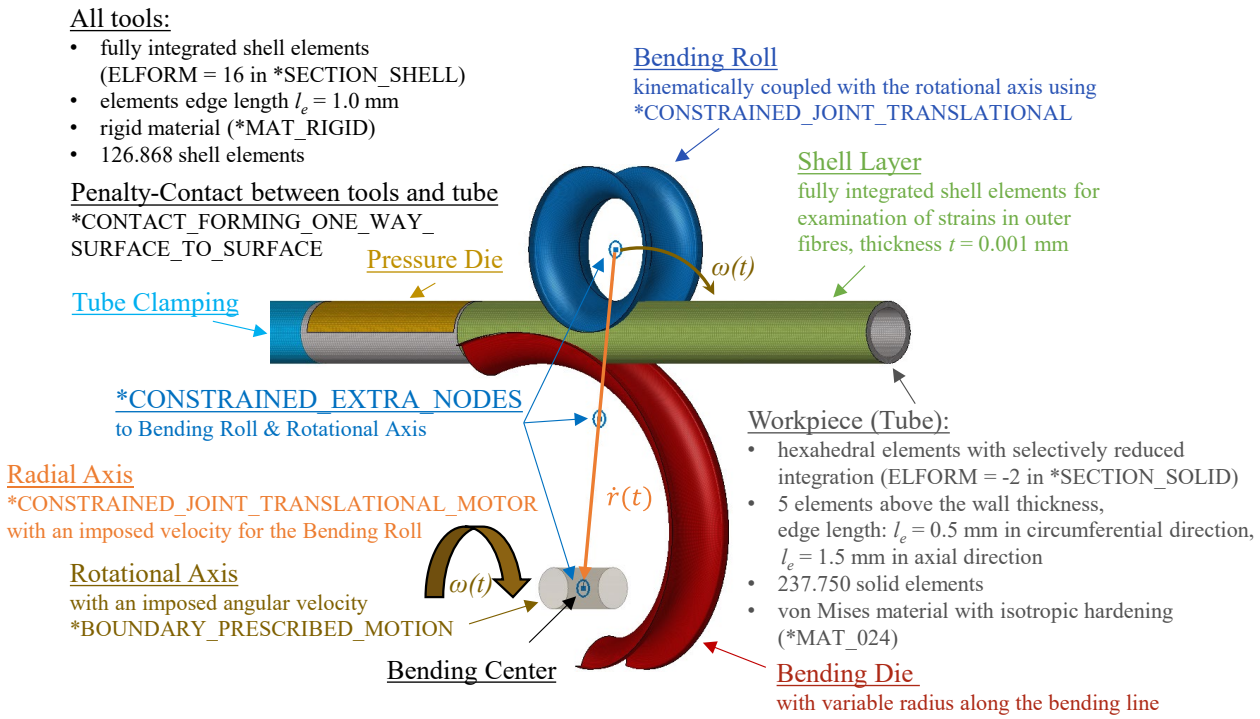

Fig. 1. FE simulation model setup based on [13, 14].

The tool surfaces are modeled as rigid bodies using shell elements with an average edge length of l_e = 1.0 mm. In total, the discretization of the tools comprises 126.868 shell elements. A rigid material model (*MAT_020) is assigned. The tube is discretized using selectively reduced, fully integrated hexahedral solid elements (ELFORM = -2 in *SECTION_SOLID). The nominal element edge lengths are set to l_e = 0.5 mm in the circumferential and l_e = 1.5 mm in the axial direction, with five elements through the wall thickness. This results in a total of 237.750 solid elements for modeling

the tube. Additionally, shell elements with a thickness of t = 0.001 mm and the same material properties as the tube are applied to the surface of the discretized tube. This approach allows for the evaluation of strains in the outer fibers.

The elastic-plastic material behavior of the tube is described using Young's modulus E, the density ρ, and the von Mises yield criterion with isotropic hardening (*MAT_024). The flow curve data are obtained from uniaxial tensile tests conducted on circular steel tubes made of E235+N, as described in detail in [13]. The experimental data are approximated using Eq. (1) following the approach proposed by El-Magd et al. [15]

$$k_f(\varphi) = C_1 + C_2 \cdot \varphi + C_3 \cdot (1 - e^{-\varphi/C_4})^n, \quad (1)$$

where k_f denotes the flow stress and φ denotes the von Mises strain. The approximation parameters C_1 to C_4 and n are determined by curve fitting using a least-squares optimization procedure.

The rotation of the bending roll about the bending center is realized in accordance with the actual process setup by introducing an additional rotational axis into the model. This axis consists of a cylindrical structure discretized with shell elements, whose center coincides with the bending center, and which is oriented perpendicular to the bending plane. The rotational axis possesses a single rotational degree of freedom about its longitudinal axis. A time-related angular velocity profile (Fig. 2) is prescribed using the *BOUNDARY_PRESCRIBED_MOTION card and applied to the rotational axis. Via a kinematic coupling implemented with *CONSTRAINED_EXTRA_NODES, this motion is transferred to the bending roll. In addition to its rotational motion, the bending roll undergoes a radial translation toward the bending center in order to follow the variable bending radius while maintaining a constant lever arm. As a result, the bending roll rotates about the bending center along a circular path with a continuously decreasing radius. The radial displacement is implemented using *CONSTRAINED_JOINT_TRANSLATIONAL, while the time-related control of the translational velocity profile (Fig. 2) is defined using the *CONSTRAINED_JOINT_TRANSLATIONAL_MOTOR card.

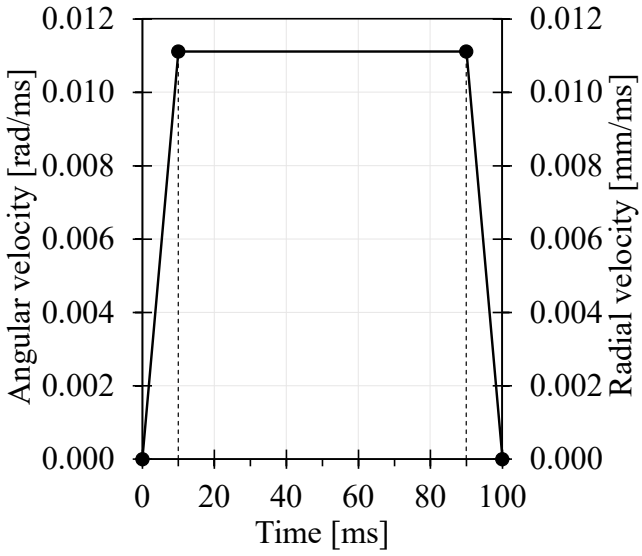

Fig. 2. Trapezoidal velocity profiles applied to the bending roll. The rise and fall times are each 10 ms. For the angular velocity, the y-scale factor in Ls-Dyna is defined as SFO = bending angle α = 1.5708 and for the radial velocity, SFO = dR/dα · bending angle α = dR/dα · 90°.

The contact interaction between the tools and the tube is described by a penalty-based numerical formulation using the *CONTACT_FORMING_ONE_WAY_SURFACE_TO_SURFACE card. In the compression bending process, no significant relative motion occurs between the tools and the tube. The tube unwraps from the bend die, while the bending roll moves along the tube surface due to its bearing-supported rotation. The pressure die and the tube clamping system remain stationary throughout the process. Accordingly, the implementation of advanced friction models is omitted, and

a Coulomb friction model is applied. The static and dynamic friction coefficients are set to $\mu_{stat} = \mu_{dyn} = 0.1$. This value is consistent with commonly reported data in tube bending literature [16, 17] and reflects the typically polished contact surfaces of bending tools, which provide only limited resistance to the initiation and continuation of sliding. For the bending roll-tube contact pair, both friction coefficients are set to zero instead of the roll's turning kinematic [13, 14]. Moreover, the aim of the simulation study is to isolate the effect of variable bend die radii on the tube deformation behavior. To this effect, the influence of roll on the tube is minimized. Consequently, friction between the bending roll and the tube is neglected to ensure that it does not affect the tube behavior associated with the variable bend die radii. The shell element thickness of the tools is neglected in the contact computation, as the elements are positioned directly on the actual tool surfaces.

Methodology

To investigate form-bound bending processes for producing tubes with variable bending radii, it is essential to understand how the geometry of a bend die with a variable contour influences the process variables and the resulting bent part quality, while accounting for the tube properties. Therefore, the present study investigates the compression bending process using bend dies with a variable radius by means of numerical simulations (Fig. 3), based on the FE model described in the preceding section.

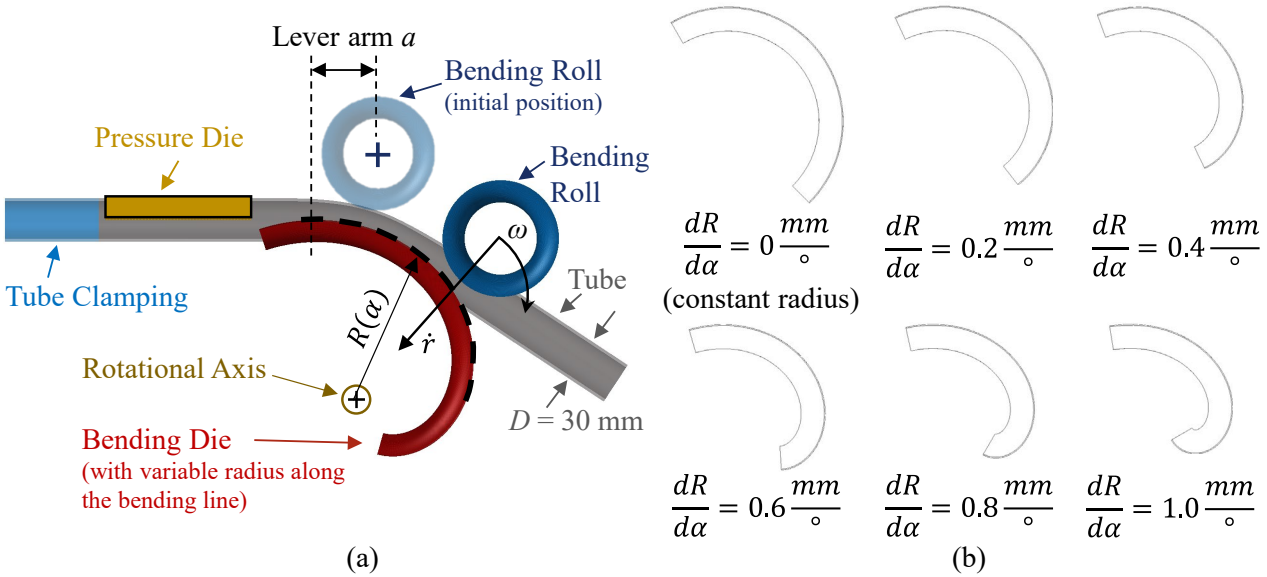

Fig. 3. Overview of the simulation study conducted to investigate the influence of the radial gradient dR/dα in compression bending using bend dies with a variable bending radius. (a) Process description of the compression bending process; (b) Schematic representation of the bend dies with a variable radius, where dR/dα = 0 mm/° denotes the constant radius.

The bend die geometry, which defines the target tube geometry during the process, is described by a continuously varying radius R(α) (Eq. (2)) following an Archimedean spiral curve [18, 19]. Starting from an initial bending radius R_0, the radius decreases continuously with increasing bending angle α at a constant radial gradient, defined as the derivative of the radius with respect to the bending angle, dR/dα. This results in a linear radius-angle relationship

$$R(\alpha) = R_0 - \frac{dR}{d\alpha} \cdot \alpha; \ \frac{dR}{d\alpha} \geq 0. \quad (2)$$

The geometry of the bend die is systematically varied according to the radial gradient dR/dα, enabling the generation of different radius profiles (Fig. 3 b). The effects of these variations on the tool reaction forces, geometrical and non-geometrical bent part properties in compression bending

are investigated. The reference case with a radial gradient dR/dα = 0 mm/°corresponds to a constant bending radius over the bending angle.

The inner radius of the bend die corresponds to the nominal inner radius of the bending task. Only circular tubes are considered. For all simulations conducted in this study, the geometric and material properties of the workpiece remain constant. The tube material is steel E235+N with an outer diameter of D = 30 mm and a constant wall thickness factor of W = D/t = 15. The initial bend factor is defined as $B_0 = R_0/D = 4$. The lever arm a = 50 mm and the bending angle α = 90° are kept constant for all parameter variations.

To evaluate the influence of the radial gradient dR/da of the bend die geometry, both process variables and the resulting geometric characteristics of the bent tubes are analyzed. The process variables considered include the tool reaction force (bending force) required during the process and the longitudinal strains in the outer and inner fibers along the extrados and intrados, respectively. The characterization of the geometric bent part features is performed based on VDI 3430 [2] and VDI 3431 [20]. The geometric characteristics include the curvature κ of the cross-sectional gravity centreline as defined in [21], the wall thickness t at the outer and inner bend, and the cross-sectional deformation of the tube, characterized by the out-of-roundness u (Fig. 4).

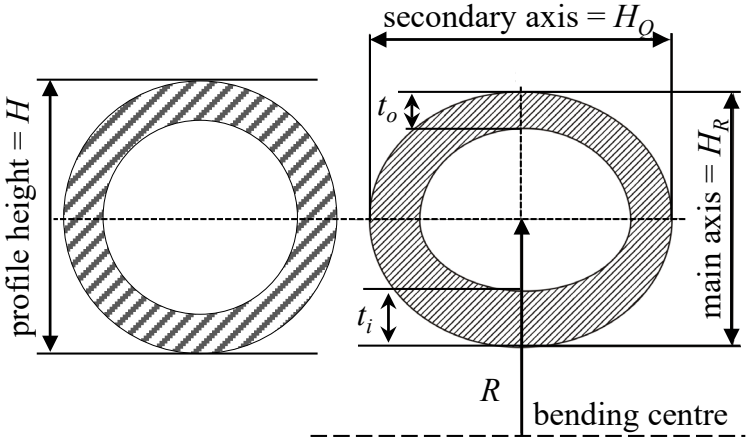

Fig. 4. Determination of the out-of-roundness u of the tube cross-section at an arbitrary position in accordance with VDI 3430 [2] and 3431 [20].

The out-of-roundness u is determined according to Eq. (3)

$$u = \frac{H_Q - H_R}{H}. \tag{3}$$

The evaluation of the geometric characteristics of the tube bends is performed automatically using a Python script analysis tool within the software Zeiss Inspect 2025, which is based on the geometry analysis tool for bent parts developed by Reuter [13]. The operational principle of this tool is described in detail in [13]. For the present study, the tool has been extended to analyze tube bends with a radius that varies along the bending angle. The main modifications concern the determination of the transition planes between the straight profile sections and the bend. These transition planes are identified based on a user-defined curvature threshold set close to zero, which defines the portion of the bend to be analyzed. The subsequent determination of characteristic parameters is carried out following the procedures described in [13].

All geometric characteristics are evaluated on non-springback tube bends. This procedure ensures an isolated assessment of the influence of varying bend die radii, such that the observed geometric variations can be attributed to differences in bend die radius, without interference from elastic recovery effects. For this purpose, the STL meshes of the bent tubes are exported during post-processing immediately after completion of the bending operation, once a bending angle of 90° has been reached, while the bending roll remains engaged.

Results

Fig. 5 illustrates the influence of the varying radial gradient dR/dα of the bend die geometry on the evolution of the bending force F_B. The bending force corresponds to the reaction force acting on the bending roll at the bending axis.

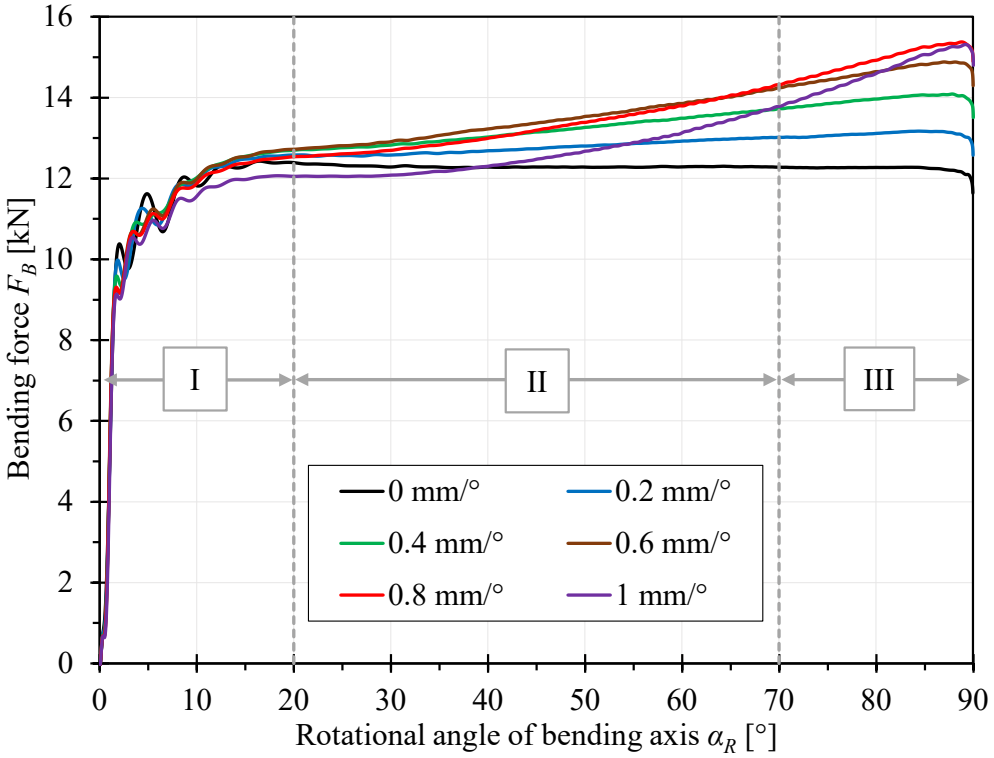

Fig. 5. Bending force F_B during compression bending using bend dies with a variable radius for different radial gradients dR/dα, plotted as a function of the rotation angle of the bending axis.

The force-angle curves show an almost identical initial increase in bending force for all investigated cases in the bend entry zone. Subsequently, the bending force increases with increasing bending angle at rates that depend on the value of dR/dα, until a maximum force is reached at the end of the bending operation. The reference case with a constant bending radius (dR/dα = 0 mm/°) exhibits the lowest maximum bending force. In general, the required bending force increases with increasing dR/dα. This effect is observed over nearly the entire bending angle range and results in an overall steeper force increase for larger values of dR/dα.

A comparison of the force evolutions reveals that the influence of dR/dα is more pronounced at medium (Fig. 5, region II) to large (Fig. 5, region III) bending angles than at small (Fig. 5, region I) bending angles, while the ranking of the force levels as a function of dR/dα is largely preserved. For dR/dα = 1 mm/°, a slightly deviating trend is observed at small to medium bending angles. Between dR/dα values of 0 mm/° and 0.6 mm/°, a continuous increase in the maximum bending force can be observed. In contrast, no significant differences in the maximum force are apparent between 0.8 mm/° und 1.0 mm/°. This behavior indicates a stagnation of the influence of a further increase in the radial gradient on the resulting bending force.

The longitudinal strains φ_L in the outer and inner fibers along the defined evaluation paths at the extrados and intrados, plotted over the normalized arc length, are shown in Fig. 6 for different values of dR/dα.

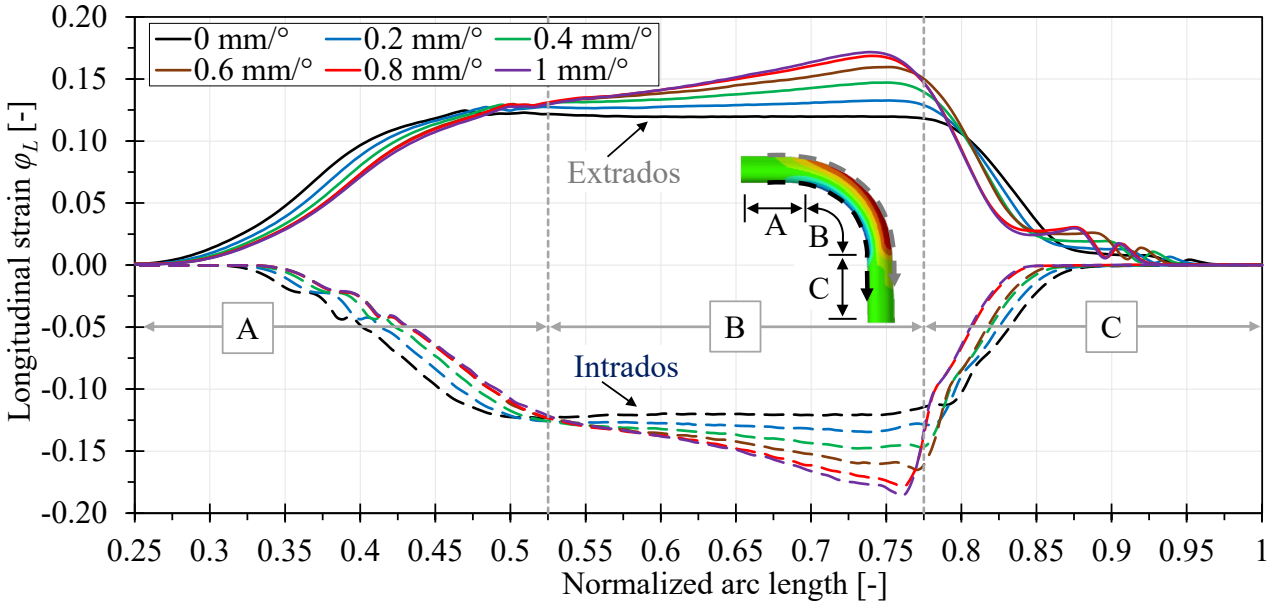

Fig. 6. Longitudinal strains φL in the outer and inner fibers along the extrados and intrados for different radial gradients dR/dα, plotted over the normalized arc length.

For the reference bend (dR/dα = 0 mm/°), the maximum longitudinal strains at both the outer and inner bend are the lowest and remain largely constant in the central bend region (Fig. 6, region B) before decreasing again in the bend exit zone (Fig. 6, region C). With increasing radial gradient dR/dα, the magnitudes of the longitudinal strains increase. At the same time, the longitudinal strains in the central bend region exhibit an approximately linear increase, with the slope becoming steeper and higher strain maxima being reached as dR/dα increases. For values above 0.8 mm/°, no significant further changes in either the strain levels or their spatial distribution along the arc length are observed, indicating a stagnation of the effect.

The phenomena observed in the process variables are also reflected in the resulting geometric characteristics. Fig. 7 presents the curvature distributions κ of the cross-sectional gravity centreline (a), the wall thickness distributions t at the inner and outer bend (b), and the out-of-roundness u of the cross-section (c), each plotted over the normalized arc length for different values of dR/dα.

For the reference bend, the curvature κ attains an almost constant value in the central bend region (Fig. 7 a, region 1). With increasing radial gradient, the curvature distributions in the central bend region increase approximately linearly, with the slope becoming steeper and higher curvature values being reached as dR/dα increases. At dR/dα = 0.6 mm/°, the maximum curvature reaches nearly 1.5 times the curvature level of the reference bend, whereas a further increase from 0.8 mm/° to 1.0 mm/° results in only a minor additional increase.

The characteristics observed in the longitudinal strain distributions (Fig. 6) are also reflected in the wall thickness distributions at the outer and inner bend (Fig. 7 b). In the reference case, only minor changes in wall thickness occur at both the outer and inner bend. With increasing dR/dα, more pronounced wall thickness variations are observed. At the outer bend, increased thinning occurs, while at the inner bend, enhanced thickening is observed. Along the arc length, the wall thickness at the outer bend decreases below, and at the inner bend increases above, the corresponding values of the reference bend (Fig. 7 b, region 1). For dR/dα > 0.8 mm/°, only minor additional changes in the wall thickness distribution are observed. Both the maximum wall thickness variations and their spatial distribution along the arc length remain largely unchanged.

The out-of-roundness u of the tube cross-section is plotted over the normalized arc length in Fig. 7 c. With increasing dR/dα, the overall level of out-of-roundness exceeds that of the reference bend. For the reference bend, the out-of-roundness remains nearly constant in the central bend region (Fig. 7 c, region 1), indicating a largely homogeneous cross-sectional deformation. For dR/dα > 0 mm/°, the out-of-roundness increases, with both the slope and the magnitude of u and thus the ovalization of the tube cross-section increasing with the radial gradient. At higher values of dR/dα,

ranging from 0.8 mm/° to 1 mm/°, the out-of-roundness distribution remains nearly unchanged, indicating a saturation of the effect.

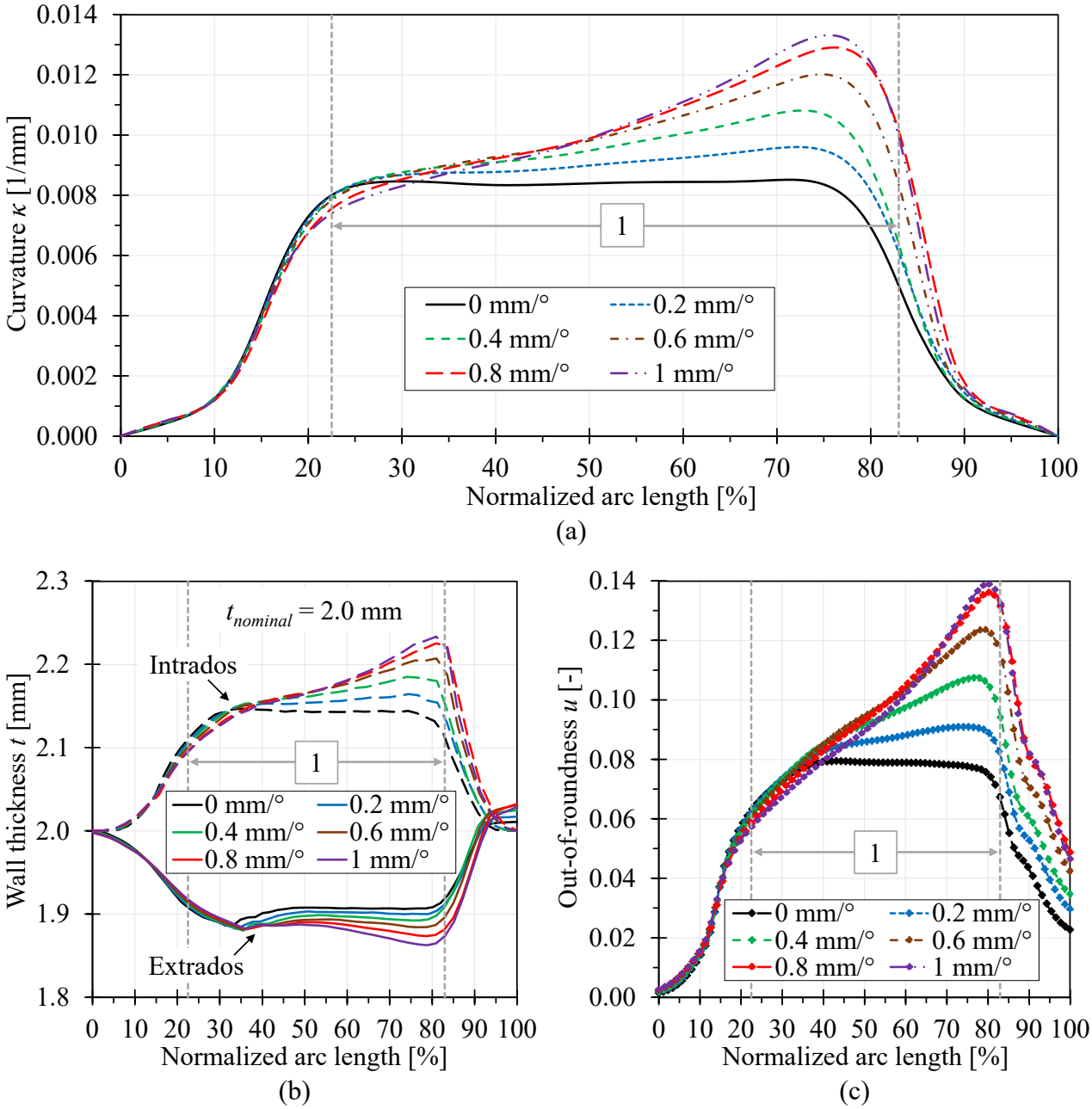

Fig. 7. Curvature κ of the cross-sectional gravity centreline (a), wall thickness t (b), and out-of-roundness u (c) for different radial gradients dR/dα, plotted over the normalized arc length.

The effects of the parameter dR/dα on the tool reaction forces, geometrical and non-geometrical bent part properties observed above are confirmed by the results shown in Fig. 8. For each quantity, the absolute maximum values are extracted and plotted as a function of the radial gradient (Fig. 8 a - e). In general, all presented quantities exhibit a pronounced linear relationship with high coefficients of determination obtained from the regression analyses ($R^2 = 0.99$) for radial gradients between 0 mm/° and 0.6 mm/°. With further increases in the radial gradient particularly from 0.8 mm/° to 1.0 mm/° a decreasing sensitivity of all investigated metrics to additional increases in dR/dα is observed.

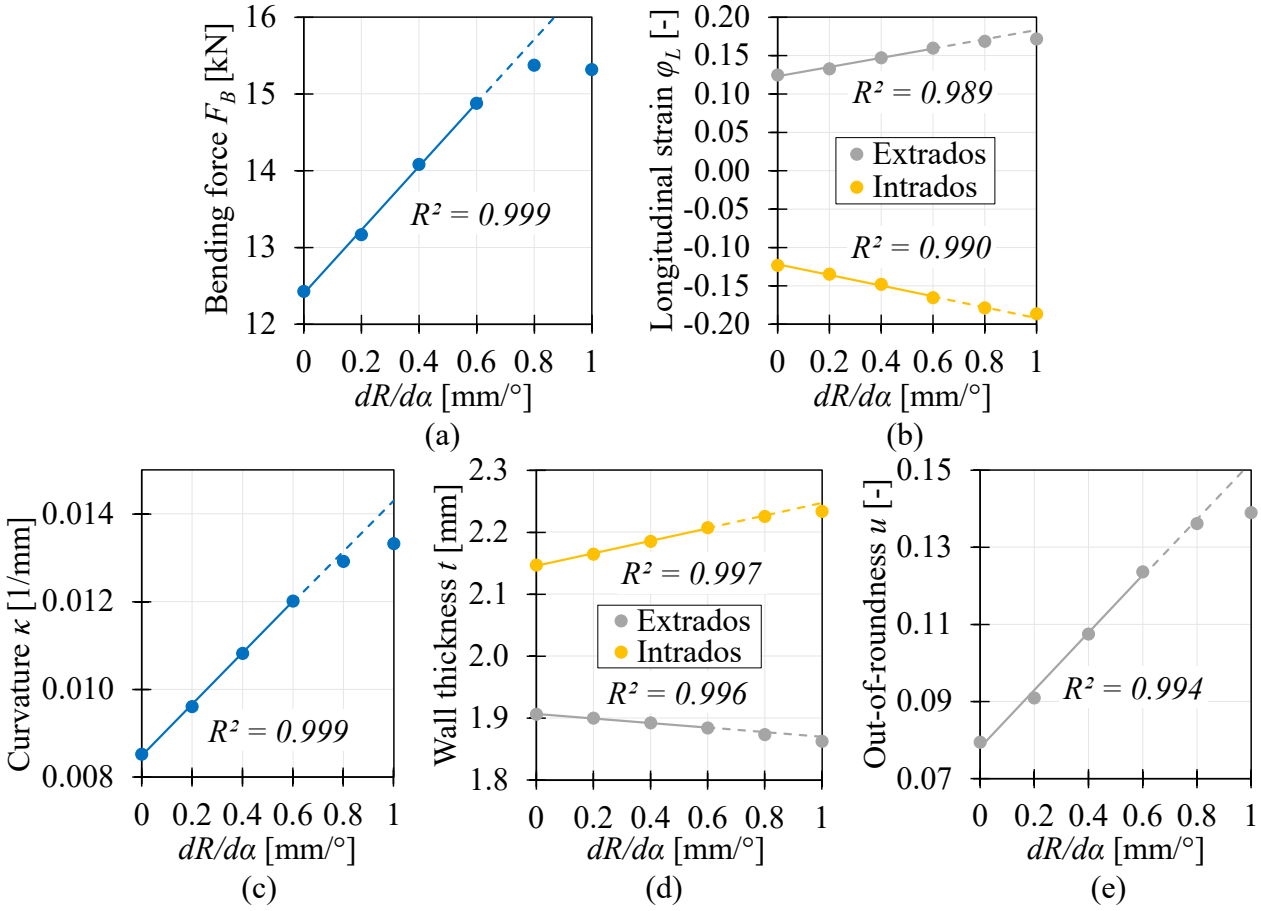

Fig. 8. Maximum values of the respective process variables and geometric characteristics for different radial gradients dR/dα.

Discussion

For radial gradients dR/dα ranging from 0 mm/° to 0.6 mm/°, linear relationships are observed between the radial gradient and the maximum values of the evaluated quantities. However, for higher radial gradient dR/dα = 0.8 mm/° and 1.0 mm/°, deviations from this linear trend become evident.

When the absolute maximum longitudinal strains φ_L at the outer bend are plotted as a function of the maximum out-of-roundness u of the tube cross-section, a strong correlation between these quantities is observed, with high coefficients of determination of the linear regression of $R^2 = 0.999$ for the outer bend and $R^2 = 0.991$ for the inner arc (Fig. 9).

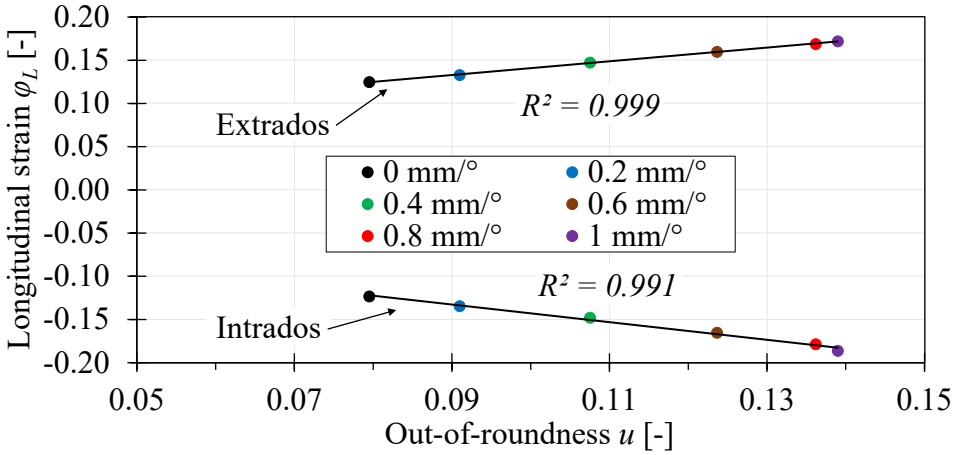

Fig. 9. Absolute maximum longitudinal strains φ_L in the outer and inner fibers along the extrados and intrados, plotted as a function of the maximum out-of-roundness u for different radial gradients dR/dα.

This indicates that beyond a certain deformation state, additional forming is preferentially accommodated by cross-sectional distortion (tube ovalization) rather than by a proportional increase in longitudinal strain. Due to the combination of wall thickness changes and the cross-sectional ovalization, a shift of the strain-neutral axis is present. Consequently, the distance between the neutral axis and the outer fiber at extrados decreases, leading to decreased longitudinal strains according to elemental bending theory. Additionally, this effect causes reduced bending stiffness, which explains the decreasing increase of bending force.

Conclusions and Outlook

In this study, the influence of bend die geometry with a continuously varying bending radius on the tool reaction forces, geometrical and non-geometrical bent part properties in compression bending was investigated for a selected bending task using FE simulations. An FE model of the compression bending process was set up, which explicitly captures the rotationally and translationally coupled kinematics of the bending roll during the process to follow the variable bending radius while keeping the lever arm constant. The bend die geometry was parameterized according to an Archimedean spiral curve, in which the radial gradient $dR/d\alpha$ was introduced as a design parameter and systematically varied from constant radius with 0 mm/° to 1 mm/°.

The results demonstrate that the feasibility of compression bending to produce tube bends with a variable radius is fundamentally given and depends on the specific bending task and the properties of the workpiece. Furthermore, the results show that the radial gradient of the bend die geometry influences the tool reaction forces and, consequently, the geometrical and non-geometrical bent part properties, with the magnitude of this influence depending on the level of the parameter.

For the bending task investigated in this study, the following conclusions can be drawn. The reference case with a constant bending radius ($dR/da = 0$ mm/°) exhibits the lowest force levels as well as the most homogeneous strain and geometric distributions within the investigated parameter range. For small to moderate values of $dR/d\alpha$ ($0 \text{ mm/°} \leq dR/d\alpha \leq 0.6 \text{ mm/°}$), a pronounced linear relationship exists between the investigated metrics and the radial gradient. This behavior is particularly evident in the representation of the maximum values as a function of $dR/d\alpha$ and is confirmed by the high coefficients of determination ($R^2 \geq 0.99$). In this parameter range, the investigated quantities respond sensitively to changes in the radius profile. An increase in $dR/d\alpha$ generally leads to higher required bending forces, increased longitudinal strains, and more pronounced geometric characteristics in terms of curvature distribution, wall thickness variation, and out-of-roundness. At high values of the radial gradient ($dR/d\alpha \geq 0.8$ mm/°), an attenuation of the effects on all considered metrics is observed. A state appears to be reached in which further geometric modifications of the bend die no longer exert a significant influence on the investigated quantities.

A possible explanation for this behavior lies in cross-section-related deformation mechanisms, such as increasing ovalization and a shift of the strain-neutral axis, which contribute to the weakening of the effects of further increases in $dR/d\alpha$. These phenomena will be analyzed in more detail in future investigations.

The FE model and numerical investigations will be experimentally validated by physical compression bending tests using bend dies with a variable bending radius for selected bending tasks. In addition, the transferability of the observed phenomena to further bending tasks and different workpiece properties will be examined.

Funding Acknowledgement

This research is part of a project funded by the Deutsche Forschungsgemeinschaft (DFG, German Research Foundation) – project number 509709804.

References

[1] F. Vollertsen, A. Sprenger, J. Kraus, H. Arnet, Extrusion, channel, and profile bending: a review, J. Mater. Process. Technol. 87 (1999) 1–27. https://doi.org/10.1016/S0924-0136(98)00339-2.

[2] VDI-Gesellschaft Produktion und Logistik, VDI 3430, Rotary draw bending of profiles: technical standard, 2014. https://www.dinmedia.de/de/technische-regel/vdi-3430/199134778.

[3] J. Cao, E. Brinksmeier, M. Fu, R.X. Gao, B. Liang, M. Merklein, M. Schmidt, J. Yanagimoto, Manufacturing of advanced smart tooling for metal forming, CIRP Ann. 68 (2019) 605–628. https://doi.org/10.1016/j.cirp.2019.05.001.

[4] D.Y. Yang, M. Bambach, J. Cao, J.R. Duflou, P. Groche, T. Kuboki, A. Sterzing, A.E. Tekkaya, C.W. Lee, Flexibility in metal forming, CIRP Ann. 67 (2018) 743 - 765. https://doi.org/10.1016/j.cirp.2018.05.004.

[5] S. Chatti, M. Hermes, A.E. Tekkaya, M. Kleiner, The new TSS bending process: 3D bending of profiles with arbitrary cross-sections, CIRP Ann. 59 (2010) 315 - 318. https://doi.org/10.1016/j.cirp.2010.03.017.

[6] S. Groth, P. Frohn, B. Engel, Product planning system for manufacture-oriented modeling of freeform bend tubes produced by three-roll-push-bending, Procedia Manuf. 34 (2019) 10 - 18. https://doi.org/10.1016/j.promfg.2019.06.107.

[7] S.A. Tronvoll, J. Ma, T. Welo, Deformation behavior in tube bending: a comparative study of compression bending and rotary draw bending, Int. J. Adv. Manuf. Technol. 124 (2023) 801 - 816. https://doi.org/10.1007/s00170-022-10433-7.

[8] W. Wang, J. Wu, L. Liu, Z. Yang, H. Wang, M. Wang, Partitioning and processing method for free-bending of spatial variable curvature tube fittings, Int. J. Adv. Manuf. Technol. 140 (2025) 2157 - 2175. https://doi.org/10.1007/s00170-025-16410-0.

[9] B. Engel, S. Kersten, D. Anders, Spline-Interpolation and Calculation of Machine Parameters for the Three-Roll-Pushbending of Spline-Contours, Steel Res. Int. 82 (2011) 1180 - 1186. https://doi.org/10.1002/srin.201100077.

[10] S. Groth, B. Engel, K. Langhammer, Algorithm for the quantitative description of freeform bend tubes produced by the three-roll-push-bending process, Prod. Eng. Res. Devel. 12 (2018) 517 - 524. https://doi.org/10.1007/s11740-018-0795-2.

[11] L. Scandola, M. Erber, P. Hagenlocher, F. Steinlehner, W. Volk, Reconstruction of the bending line for free-form bent components extracting the centroids and exploiting NURBS curves, Graph. Models 135 (2024) 101227. https://doi.org/10.1016/j.gmod.2024.101227.

[12] M. Elyasi, F.A. Khatir, H. Talebi Ghadikolaee, V. Modanloo, Experimental investigation and numerical simulation of the effect of type of bending die on the quality of tube forming in rotary draw bending process, Int. J. Lightw. Mater. Manuf. 7 (2024) 233 - 247. https://doi.org/10.1016/j.ijlmm.2023.10.005.

[13] J. Reuter, Methode zur Gestaltung segmentierter Werkzeuge für die Flexibilisierung von Biegeprozessen Jonas Reuter, universi - Universitätsverlag Siegen, Siegen, 2025.

[14] J. Mrochen, J. Reuter, A. Aslanidis, P. Frohn-Sörensen, L. Hansmann, B. Engel, U. Lorenz, Topology optimized metal forming tools: Using Mixed-Integer Programming to design truss-like structures (2025). https://doi.org/10.21203/rs.3.rs-7021236/v1.

[15] E. El-Magd, C. Treppman, M. Korthäuer, Description of flow curves over wide ranges of strain rate and temperature, Int. J. Mater. Res. 97 (2006) 1453 - 1459. https://doi.org/10.3139/146.101390.

[16] P. Frohn-Sörensen, C. Cislo, H. Paschke, M. Stockinger, B. Engel, Dry friction under pressure variation of PACVD TiN surfaces on selected automotive sheet metals for the application in unlubricated metal forming, Wear 476 (2021) 203750. https://doi.org/10.1016/j.wear.2021.203750.

[17] M.A. Kaleem, R. Steinheimer, P. Frohn-Sörensen, T. Kotzian, B. Engel, Topology optimization of forming tools: pressure die in rotary draw bending process, Int. J. Interact. Des. Manuf. 19 (2025) 3349 - 3362. https://doi.org/10.1007/s12008-024-01932-w.

[18] A. Polezhaev, Spirals, Their Types and Peculiarities, Spirals and Vortices (2019) 91 - 112. https://doi.org/10.1007/978-3-030-05798-5_4.

[19] F. Kürpig, O. Niewiadomski, Spiralen, in: F. Kürpig, O. Niewiadomski (Eds.), Grundlehre Geometrie: Begriffe, Lehrsätze, Grundkonstruktionen, Vieweg+Teubner Verlag, Wiesbaden, 1992, pp. 79 - 84.

[20] VDI-Gesellschaft Produktion und Logistik, VDI 3431, Bending of profiles: testing notes for profile bending elements, technical standard, 2016. https://www.dinmedia.de/de/technische-regel/vdi-3431/257014788.

[21] M.P.d. Carmo, Differential geometry of curves and surfaces, Revised & updated second edition, Dover PublicationsInc, Mineola, New York, 2016.